

Highly Collimated Jets and Wide-Angle Outflows in HH46/47: New Evidence from Spitzer IR Images

T. Velusamy¹, William D. Langer¹, Kenneth. A. Marsh^{1,2}

ABSTRACT

We present new details of the structure and morphology of the jets and outflows in HH46/47 as seen in Spitzer infrared images from IRAC and MIPS, reprocessed using the “HiRes” deconvolution technique. HiRes improves the visualization of spatial morphology by enhancing resolution (to sub-arcsec levels in IRAC bands) and removing the contaminating side lobes from bright sources. In addition to sharper views of previously reported bow shocks, we have detected: (i) the sharply-delineated cavity walls of the wide-angle biconical outflow, seen in scattered light on both sides of the protostar, (ii) several very narrow jet features at distances ~ 400 AU to ~ 0.1 pc from the star, and, (iii) compact emissions at MIPS $24\ \mu\text{m}$ coincident with the jet heads, tracing the hottest atomic/ionic gas in the bow shocks. Together the IRAC and MIPS images provide a more complete picture of the bow shocks, tracing both the molecular and atomic/ionic gases, respectively. The narrow width and alignment of all jet-related features indicate a high degree of jet collimation and low divergence (width of ~ 400 AU increasing by only a factor of 2.3 over 0.2pc). The morphology of this jet, bow shocks, wide angle outflows, and the fact that jet is non-precessing and episodic, constrain the mechanisms for producing the jet’s entrained molecular gas, and origins of the fast jet, and slower wide-angle outflow.

Subject headings: ISM: jets and outflows — ISM: Herbig-Haro objects — stars: formation — ISM: individual (HH46/47)

1. Introduction

Protostellar jets and winds originate close to the surface of the forming star and interact with the dense envelope surrounding the protostar-disk system (Königl & Pudritz 2000; Shu

¹Jet Propulsion Laboratory, Pasadena, CA 91109; velusamy@jpl.nasa.gov

²IPAC, Caltech, Pasadena, CA 91125

et al. 2000). Both wide angle outflows and collimated jets from young protostars play an important role in how stars form, as they provide a means for protostellar disks to shed material and angular momentum, thus regulating stellar mass via accretion of disk material onto the star. HH46/47 is a remarkable example of a system with jets and bow shock cavities, and, as reported here, wide angle outflow cavities, offering a rich observational insight into the various mechanisms at play (Reipurth & Heathcote 1991; Chernin & Masson 1991; Eislöffel et al. 1994, Combet et al. 2006). The jets in HH46/47 are bright and show a classic structure of a collimated flow with several large bow shocks (HH47A, HH47C, HH47D). Recently, the HH46/47 system was observed by Spitzer with the IRAC, IRS, and MIPS instruments as part of the Early Release Observations, and the results were presented by Noriega-Crespo et al. (2004) and Raga et al. (2004). In the IRAC bands, they clearly detect the bow shock and its cavities; these IR emissions arise from the the H_2 rotational lines and possibly some contribution from PAHs. However, in these images many of the features in both the IRAC and MIPS data are overwhelmed by the diffraction lobes from the very bright central source. Here we present new results for HH46/47 based on reprocessing the IRAC and MIPS Spitzer archive data using a deconvolution algorithm. The “HiRes” deconvolution developed for Spitzer images by Backus et al. (2005) is based on the Richardson-Lucy algorithm (Richardson 1972; Lucy 1974), and the Maximum Correlation Method (Aumann et al. 1990) used for IRAS data. HiRes deconvolution improves the visualization of spatial morphology by enhancing resolution (to sub-arcsec levels in the IRAC bands) and removing the contaminating sidelobes from bright sources (Velusamy et al. 2007a & 2007b).

2. Results

In Figs. 1-3, we present the HiRes deconvolved images of HH46/47 in all IRAC bands and in MIPS $24\ \mu\text{m}$ using the data in Spitzer archives. For comparison the diffraction-limited “mosaic” images are also shown in Fig. 1. The effects of the resolution enhancement (e.g. from $2''.4$ to $\sim 0''.8$ at $8\ \mu\text{m}$) and the removal of the diffraction lobes (with residues near the Airy rings at a level $< 0.05\%$ of the peak intensity) are clearly evident in these images. A wide-angle outflow cavity is now clearly detected in scattered light in the 3.6 and $4.5\ \mu\text{m}$ images, while the bow shocks and their limb brightened cavities appear prominently in all IRAC bands. At $24\ \mu\text{m}$, we detect only the central protostar and two compact sources near the tip of the bow shocks (Figs. 1 & 3). In Fig. 2 we show a blow up of the emissions in IRAC channels 1-2 near the protostar. A composite view of the overall morphology and identification of the individual components of the HH46/47 outflow/jet system is shown in Fig. 3. SEDs of selected features are shown in Fig. 4.

2.1. Collimated jets: The most significant result of our HiRes processing is the jet morphology. In the SW, we observe well-collimated jet features on all distance scales from the protostar, up to its termination at the head of the bow shock HH47C (24 μ m hotspot). In the NE the most remarkable jet feature is the 24 μ m hotspot at the jet impact site in the bow shock HH47A. Here we do not observe any other jet emission features toward the bowshock, unlike the case of the SW jet. The emission features along the SW jet characterize its collimation and quantify its divergence: (i) closest to the protostar it appears as a protrusion representing the entrained molecular jet closest to its base (Fig. 2). (ii) a remarkably very narrow $\sim 1'' - 1.5''$ wide, and $\sim 10''$ long “compact jet” (Figs. 2 & 3), is seen at $15''$ from the protostar. Its long axis is perfectly aligned with the star and 24 μ m hotspot (Fig. 3). This feature is also visible in the H₂ images of Eislöffel et al (1994). Our HiRes IRAC images fully resolve the jet along, and perpendicular to, its velocity axis (Fig. 2c). We estimate a radius of ~ 300 AU for the entrained molecular jet at 9000AU from the star (at distance 450 pc). (iii) a feature $\sim 10''$ (4,500 AU) from the star which is coincident with an optical knot in the HST NIC2 image (Reipurth et al. 2000) and a compact feature in the H₂ image (Eislöffel et al. 1994). (vi) a feature at $\sim 50''$ (0.1 pc) from the star is aligned well with the SW jet although we cannot exclude that it is a part of the bow shock seen in projection.

The most prominent jet features in the HiRes 24 μ m image are the “hotspots” in the SW & NE bow shocks. These emissions were noted in the mosaic images by Noriega-Crespo et al (2004). Here we discuss their morphology using the HiRes deconvolution and their relationship to the jets and bow shocks. In the IRAC bands the emissions from the bow shocks delineate long arcs that extend to large distances backwards from the jet heads to the protostar. The emissions in the IRAC bands are considered to be from pure rotational H₂ lines excited by C-shocks (Neufeld et al. 2006). In contrast, the MIPS 24 μ m emissions appear to be coincident with the head of the jets, representing emission generated by shocks in a Working Surface (WS). They are compact and somewhat more extended perpendicular to the jet $\sim 2''.2 \times 2''.8$ and $3''.0 \times 5''.9$ axis, sizes for the SW (HH47C) and NE (HH47A) hotspots, respectively. The morphology of the 24 μ m emission (possibly from the J-shock in the WS) is distinctly different from that associated with the molecular shocks (C-shocks) extending further back. The SEDs of these hotspots show clear 24 μ m excess in contrast to that along the bow shock (Fig. 4). The optical (Hartigan et al. 1990) and IR (Noriega-Crespo et al. 2004) spectra in HH47A show only strong atomic/ionic lines and no continuum. We can therefore rule out the MIPS 24 μ m emission as due to warm dust and instead it originates in the hottest gas in the bow-shock. In the IRS spectrum of HH47A (Fig. 6 in Noriego-Crespo et al. 2004) bright [FeII] line emissions at 24.51 μ m and 25.98 μ m lie within the MIPS 24 μ m passband. Indeed, the faint emission (~ 10 mJy) in the MIPS 24 μ m image is consistent with these line intensities considering the respective widths of the lines and the MIPS 24

μm pass band. Thus both the NE and SW $24\ \mu\text{m}$ hotspots can be regarded as tracing the hottest atomic/ionic gas in the bow shocks and therefore they identify the current impact location of the jet with the ambient envelope.

We use the multiple emission features along the SW jet to estimate the divergence of the jet. The compact jet at $20''$ (9,000 AU) from the star has a width of $1''.1$ perpendicular to the jet and the hotspot at a distance of $116''$ (0.25 pc) has a width of $2''.8$. Taking into consideration the HiRes beams we estimate the divergence of the jet entrained molecular material is a factor of ~ 2.3 over a distance $96''$ ($\sim 0.21\text{pc}$). This divergence of the jet (an increase in radius, ~ 290 AU at $24\ \mu\text{m}$ hotspot), indicates an expansion at $1.8\ \text{kms}^{-1}$ perpendicular to the jet, assuming a typical jet velocity of $\sim 250\ \text{kms}^{-1}$ (Eisloffel, & Mundt, 1994). This expansion velocity is consistent with free expansion of the molecular gas transverse to the jet axis at the co-moving sound speed ($\sim 2\text{kms}^{-1}$ for H_2 at $T_{\text{gas}} \sim 10^3\ \text{K}$). Thus, assuming no external confinement, the jet has remained highly collimated over $\sim 0.2\ \text{pc}$ (up to its impact with the surrounding envelope). The spatially discrete emissions along the jet axis suggests the jet activity is episodic and is consistent with the larger parsec scale outflows observed in HH46/47 (Stanke et al. 1999). The alignment of the knots, and the jet head and the linear morphology of the compact jet rules out a precessing jet.

2.2. Wide-angle outflows: The wide angle outflows are clearly detected in the 3.6 and $4.5\ \mu\text{m}$ HiRes images (Figs. 1 - 3) and this is the first evidence of a bipolar (NE & SW) wide-angle outflow cavity in HH46/47 as observed in the scattered light from the protostar. The optically observed parabolic sheath of reflection nebulosity towards the NE (Reipurth et al. 2000) traces parts of this outflow, which is also observed in all IRAC bands. However, the scattered light at 3.6 and $4.5\ \mu\text{m}$ traces a much wider outflow (Figs. 2 & 3). The NE outflow lobe is clearly a mix of an inner bright parabolic cavity traced in both reflected light and entrained molecular gas, and a broader wide-angle component detected only in scattered light at $3.6\ \mu\text{m}$. The wide-angle outflow cavity towards the SW is not detected in the optical, possibly due to its faintness and the viewing geometry and it may be hidden behind ambient cloud material (Stanke et al. 1999). With this new detection of the wide-angle outflow to the SW (apparent opening angle of $\sim 110^\circ$), HH46/47 emerges as a classical example of an wide-angle outflow - narrow jet system, placing it among those with very wide outflows (Velusamy & Langer 1998; Arce & Sargent 2006). It would be interesting if such wide opening angles in HH46/47 is the result of outflow evolution with age as proposed by Velusamy & Langer (1998). Since outflows can disperse the envelope and modify the infall geometry, this provides a natural mechanism to stop the infall, ending the accreting phase.

3. Discussion

Our HiRes deconvolved Spitzer images of HH46/47 show the concurrent presence of both highly collimated fast bipolar jets and poorly collimated slower wide-angle outflow. The cool molecular gas in the wide-angle outflow (because it does not emit in other IR bands, unlike the jet or the bow shock) is observed along with the presence of warmer entrained molecular gas along the jet close to the protostar (within $1''$ – $2''$). The magnetocentrifugal origin of jets and their launch from the magnetized accretion disk of the protostar (Ouyed & Pudritz 1997) are generally accepted, although the detailed mechanism is under debate. In contrast, the wide angle outflow may be jet driven (Raga & Cabrit 1993, Ostriker et al. 2001) or wind driven (Shu et al. 2000). In the jet driven model the bow shock produces a thin shell that stretches out from the jet head back to the star (Fig. 3). The models of Raga et al. (2004) for HH47C have a leading bow shock with wings extending all the way back to the protostar producing a dense shell of material. However, this bow shock bubble is much narrower than the wide-angle outflow traced by scattered light (Fig. 3). Clearly, the wide angle outflow is not part of this bow shock and we can rule out a jet-driven origin. The wide angle outflow alone can be explained by wind-driven models. Another possible scenario for the jet and outflow structure in HH46/47 is an MHD self-similar model (Lery 2003, Combet et al. 2006) where radiation and magnetocentrifugal acceleration and collimation produce heated pressure-driven outflows. Here, in addition to a central accretion-ejection engine driving the atomic jet, the wide-angle molecular outflow is powered by the infalling matter that follows a circulation pattern around the central object without necessarily being entrained by the jet (Figs. 4 & 7 in Combet et al. 2006). The molecular outflows appear as a wider hollow conical structure. The central jet is atomic and occupies the axial region. In this scenario, there is no strong relation between the fast jet and the slower molecular wide angle outflow near the protostar.

In HH46/47 the SW jet is propagating inside a bubble (created by the bow shock) and there is little chance for molecular gas entrainment along its path. Therefore, the detection of the jet features in the molecular gas (IRAC bands) all along the jet axis towards the bow shock, indicate that substantial molecular gas entrainment in the jet must have occurred right at the base of the jet. We estimate a size ~ 300 AU for the entrained molecular jet at its base near the star, obtained by extrapolating back to the star the divergence of the molecular jet between the compact jet and the jet head at HH47C, (section 2.1). In other words, the atomic jet which originates within a few AU of the star must have entrained the molecular gas within the star-disk-infall interface region which is at least 300 AU across. Thus, our results constrain the density structure above the base of the atomic jet in such a way that sufficient molecular material is still available to the jet to entrain molecular gas across a few hundred AU before it enters the cavity created by the wide-angle outflow and

bowshocks. The molecular gas entrainment along the atomic jet occurs at least up to a few hundred AU from the star into the star-disk-infall interface. Such gas entrainment by the jet is possible, for example, in the models by Combet et al (2006) where the infall-outflow circulation provides a molecular gas buffer over a few hundred AU across and above the star. This material near the vertex of the outflow cones is sufficient for the atomic jet emerging from below to entrain molecular gas as observed in HH46/47.

We thank the referee for helpful suggestions regarding the interpretation of the 24 μm emission. The research described in this paper was carried out at the JPL, Caltech, under a contract with NASA. We thank Timothy Thompson for his help with the data analysis.

REFERENCES

- Aumann, H. H., Fowler, J. W. & Melnyk, M., 1990 AJ, 99, 1674
- Arce, H. G., & Sargent, A. I. 2006, ApJ, 646, 1070
- Backus, C.R. , Velusamy, T., Thompson, T.J. and Arballo, J.K., 2005, in ADASS XIV, ASP Conference Series, Vol. 347, p 61
- Chernin, L., & Masson, C. R. 1991, ApJ, 372, 646
- Combet, C., Lery, T., Murphy, G.C. 2006, ApJ 637,798
- Eisloffel, J., Davis, C. J., Ray, T. P., & Mundt, R. 1994, ApJ, 422, L91
- Eisloffel, J., & Mundt, R. 1994, A&A, 284, 530
- Hartigan, P., Raymond, J., & Meaburn, J. 1990, ApJ, 362, 624
- Königl A. and Pudritz R. E. (2000) In Protostars and Planets IV, p 759
- Lery, T, 2003 Astrophys & Space Science 287, 35
- Lucy, L. B., 1974 AJ, 79, 745
- Neufeld, D.A. et al. 2006, ApJ, 649, 816
- Noriega-Crespo, A., et al. 2004, ApJS, 154, 352
- Ostriker, E. C., Lee, C., Stone, J. M., & Mundy, L. G. 2001, ApJ, 557, 443

- Ouyed, R., & Pudritz, R. E. 1997, *ApJ*, 482, 712
- Raga, A., & Cabrit, S. 1993, *A&A*, 278, 267
- Raga, A. C., Noriega-Crespo, A., Gonzalez, R. F., & Velazquez, P. F. 2004, *ApJS*, 154, 346
- Reipurth, B., & Heathcote, S. 1991, *A&A*, 246, 511
- Reipurth, B., Yu, K., Heathcote, S., Bally, J., & Rodriguez, L. 2000, *AJ*, 120, 1449
- Richardson, W. H., 1972 *J. Opt. Soc. Am.*, 62, 55
- Shu, F. H., Najita, J. R., Shang, H., & Li, Z.-Y. 2000, in *Protostars and Planets IV*, p 789
- Stanke, T., McCaughrean, M. J., & Zinnecker, H. 1999, *A&A*, 350, L43
- Velusamy, T., Marsh, K.A., Beichman, C.A., Backus, C.R., Thompson, T.J. 2007 (submitted to *AJ*)
- Velusamy, T., Langer, W.D., Marsh, K.A. 2007 *BAAS* 39, 198
- Velusamy, T. & Langer, W.D. 1998, *Nature*, 392,685

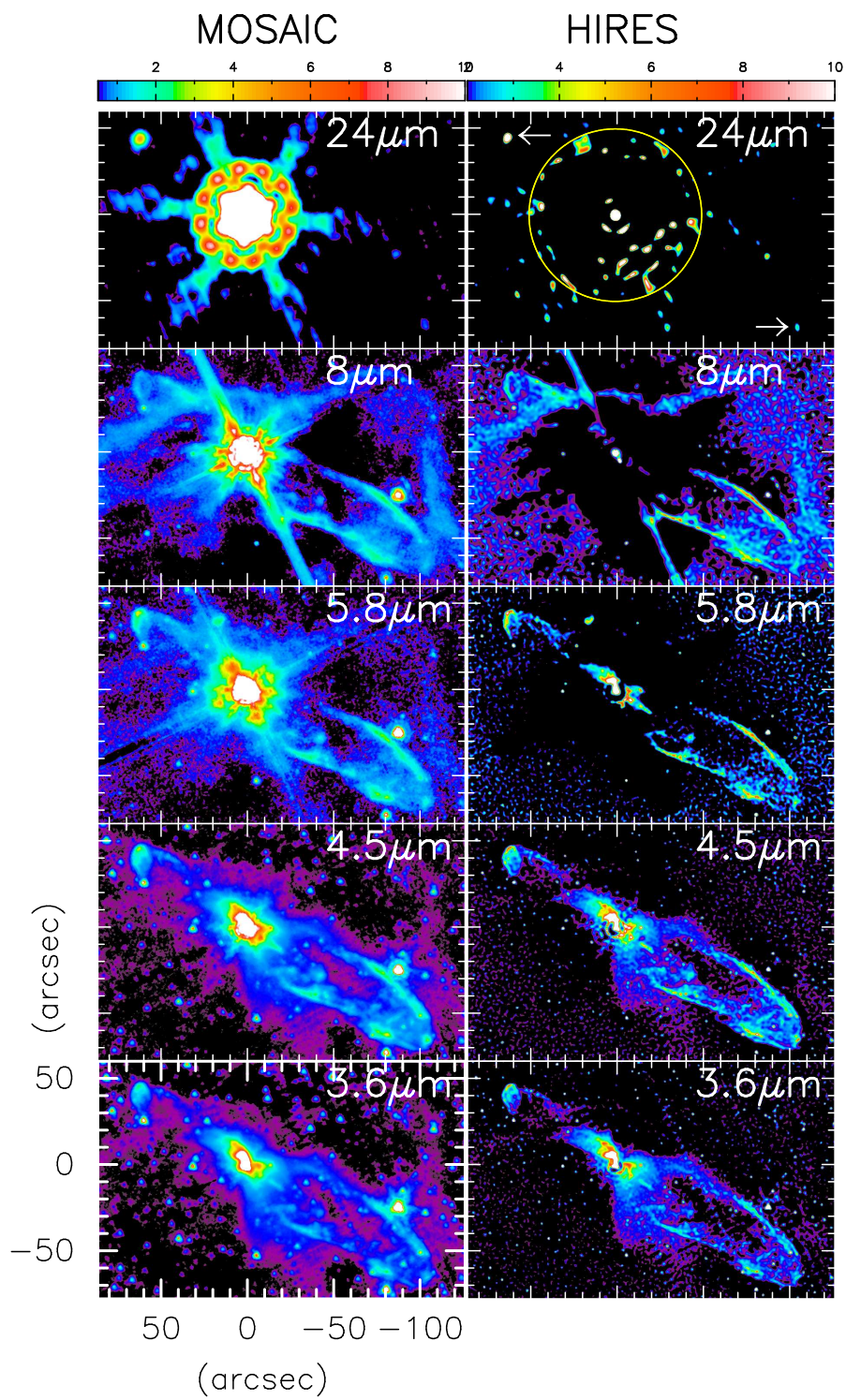


Fig. 1. The Messier 1 (left) and HiRes-deconvolved (right) Spitzer IRAC and MIPS images.

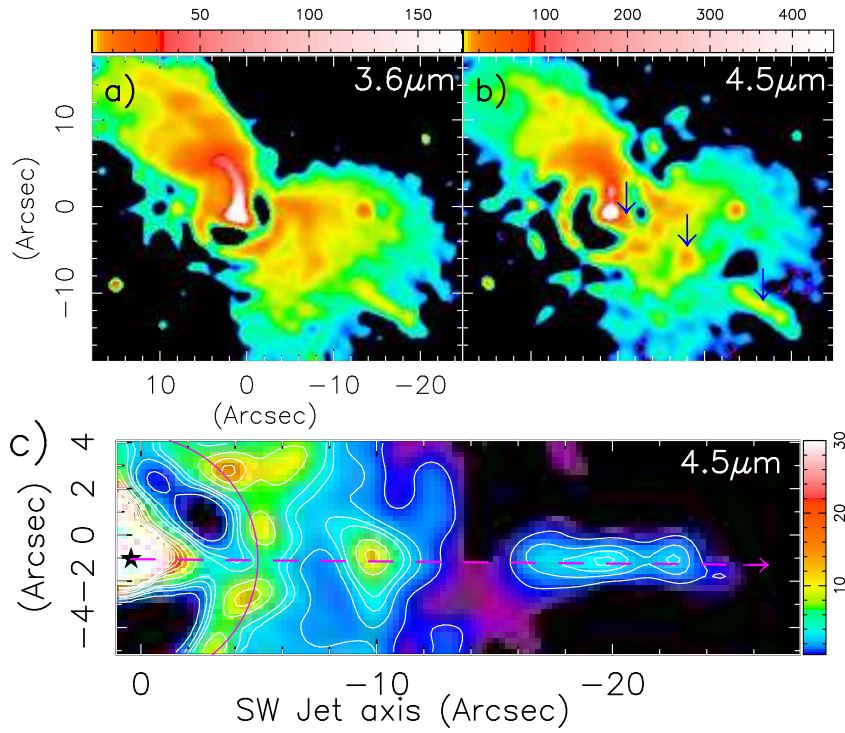


Fig. 2.— (a) and (b) HiRes deconvolved images of the region around the protostar (HH46 IRS) at 3.6 and 4.5 μm . Log color stretch is used with highest intensities at the 20% and 4%, level of the protostar peak brightness at 3.6 and 4.5 μm , respectively. The lowest surface brightness (indicated by blueish green) traces the wide angle outflows to the NE and SW. The black arrows in (b) mark the jet-like protrusion, H₂ knot, and the compact jet which are well aligned with the SW jet (Fig. 3). The circular arc marks the residue in the airy lobe at a level of 0.04% of the peak ($1.2 \times 10^4 M J y s r^{-1}$). (c) IRAC 4.5 μm contour map and the gray scale image of the jet features along the SW lobe. The contours are at 1, 2, 3, 4, 8, 12, 32 $M J y s r^{-1}$. The star symbol and dashed lines mark the protostar and the jet axis.

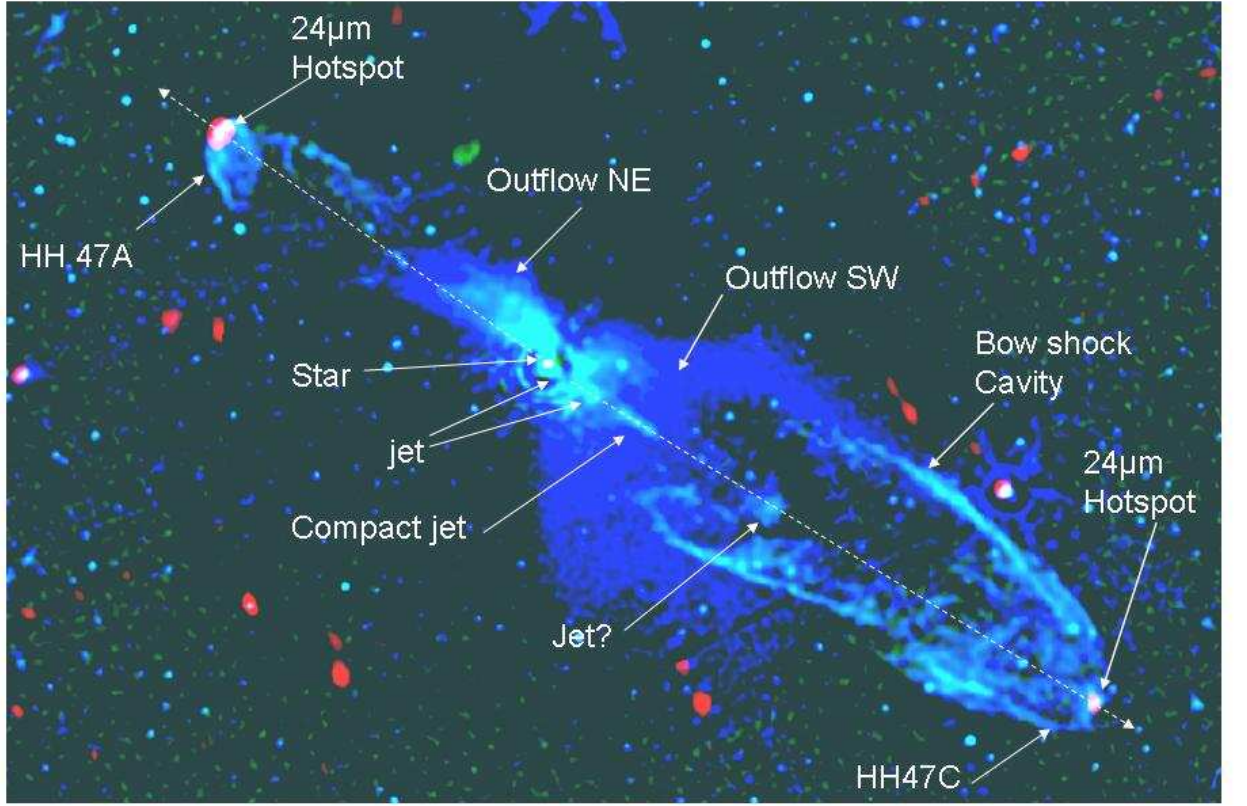


Fig. 3.— HiRes deconvolved three-color Spitzer images: IRAC 3.6 μm (blue), IRAC (4.5 μm + 5.8 μm) (green), MIPS 24 μm (red). To avoid confusion, the diffraction residue around the protostar in the 24 μm image inside the circle in Fig.1 is not shown. The labels identify the observed features described in the text.

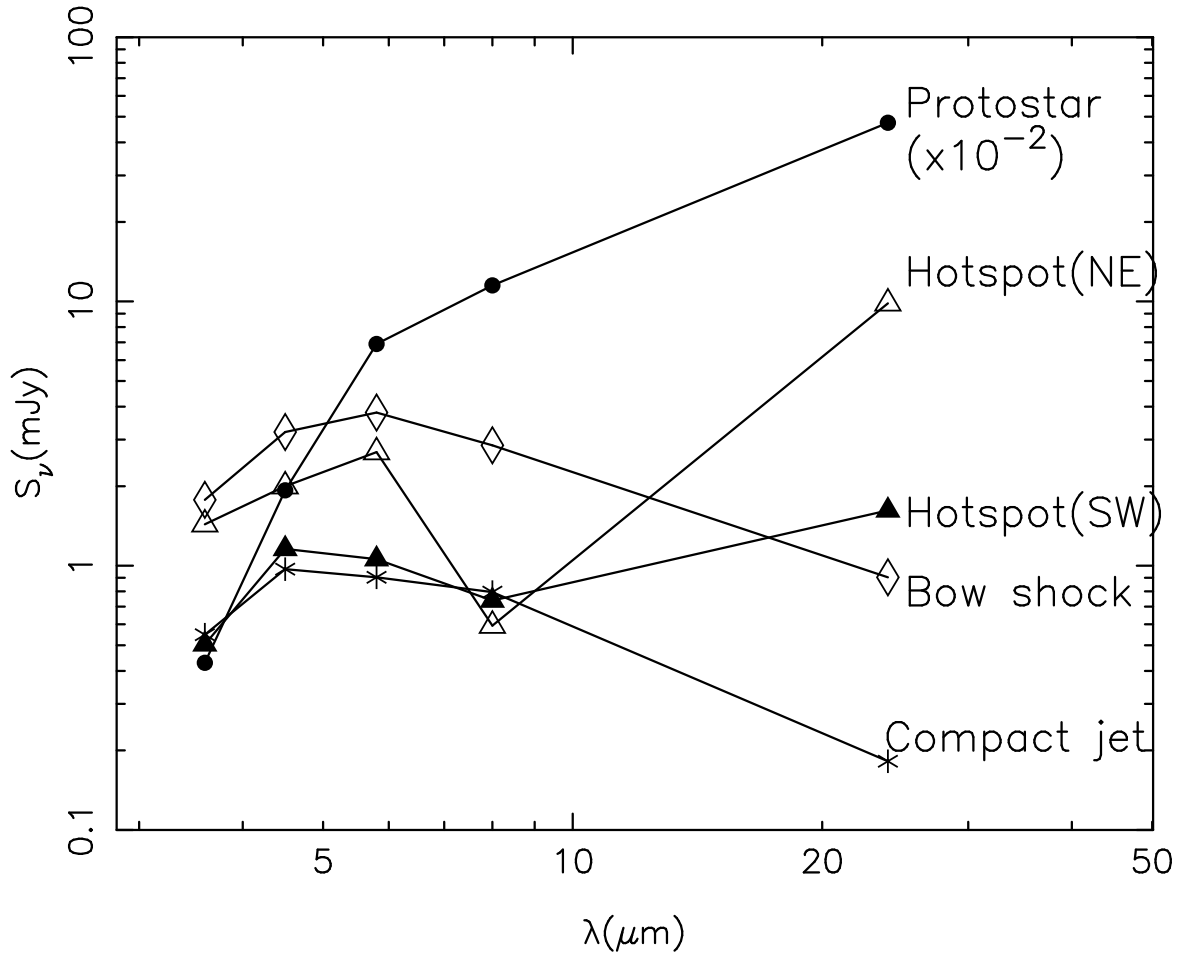


Fig. 4. SEDs at the positions marked in Fig. 2. The SNRs for the fluxes are ≥ 8 at all